# Dynamics of Azobenzene Dimer Photoisomerization: Electronic and Steric Effects

Evgenii Titov,[†] Giovanni Granucci,[‡] Jan Philipp Götze,[†] Maurizio Persico,[‡] and Peter Saalfrank[*,†]

*Theoretical Chemistry, Institute of Chemistry, University of Potsdam, Karl-Liebknecht-Str. 24-25, 14476 Potsdam, Germany, and Department of Chemistry and Industrial Chemistry, University of Pisa, via Moruzzi 13, 56124 Pisa, Italy*

E-mail: peter.saalfrank@uni-potsdam.de

[*]To whom correspondence should be addressed

[†]Theoretical Chemistry, Institute of Chemistry, University of Potsdam, Karl-Liebknecht-Str. 24-25, 14476 Potsdam, Germany

[‡]Department of Chemistry and Industrial Chemistry, University of Pisa, via Moruzzi 13, 56124 Pisa, Italy

## Abstract

While azobenzenes readily photoswitch in solution, their photoisomerization in densely packed self-assembled monolayers (SAMs) can be suppressed. Reasons for this can be steric hindrance and/or electronic quenching, *e.g.*, by exciton coupling. We address these possibilities by means of nonadiabatic molecular dynamics with trajectory surface hopping calculations, investigating the *trans* $\rightarrow$ *cis* isomerization of azobenzene after excitation into the $\pi\pi^*$ absorption band. We consider a free monomer, an isolated dimer and a dimer embedded in a SAM-like environment of additional azobenzene molecules, imitating in this way the gradual transition from an unconstrained over an electronically coupled to an electronically coupled and sterically hindered, molecular switch. Our simulations reveal that in comparison to the single molecule the quantum yield of the *trans* $\rightarrow$ *cis* photoisomerization is similar for the isolated dimer, but greatly reduced in the sterically constrained situation. Other implications of dimerization and steric constraints are also discussed.


**TOC graphic:**

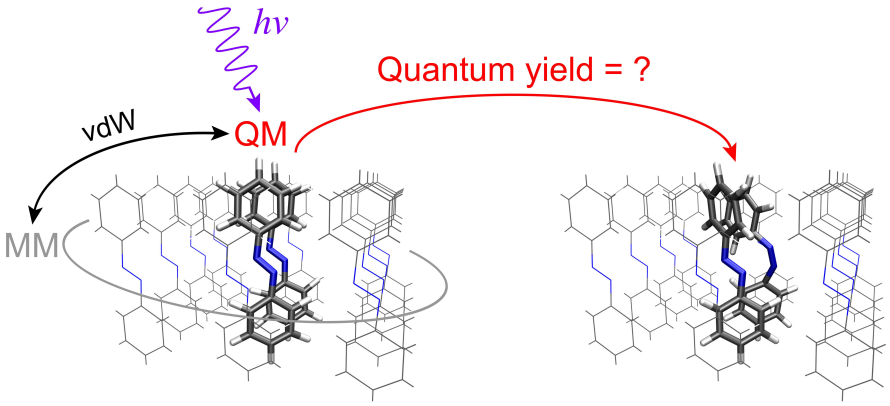

The photoswitching of an azobenzene (AB) molecule between two different isomers, *trans* and *cis*, is a widely studied example of molecular switching which is of importance to potential applications in nanoscience. Readily accessible in gas phase or solution, the *trans* $\rightarrow$ *cis* photoisomerization can be hindered in densely packed self-assembled monolayers (SAMs), as has been observed for AB-containing thiols on a gold surface.[1,2] As possible reasons for this suppression of the isomerization, steric hindrance and/or large exciton coupling between AB chromophores, leading to ultrafast excitation transfer in the SAM, have been mentioned.[1] However, thorough insight into details of the problem is still elusive.

Since steric and electronic effects are hard to disentangle experimentally, theoretical modeling is worthwhile. Here in particular nonadiabatic molecular dynamics appears as a powerful tool to gain mechanistic insight into multi-mode, photoinduced molecular switching. So far, nonadiabatic molecular dynamics with trajectory surface hopping was applied to model single-molecule isomerization of AB in gas phase,[3–12] in solution,[5,6] and in the liquid state.[10,11] The isomerization of (single) AB derivatives on sterically confining surfaces was also modeled showing a reduction of the quantum yield of reaction in comparison to the isolated-molecule case due to van der Waals (vdW) interation with a surface and resulting steric hindrance.[13,14] Furthermore, covalently connected dimeric molecular systems with two AB units, were considered either in quantum mechanics / molecular mechanics (QM/MM)[15] or purely QM[16] (regarding the electronic structure) setups.

In this work we make a step further, simulating by means of the surface hopping approach[17,18] with QM and QM/MM models the *trans* $\rightarrow$ *cis* isomerization dynamics of a non-covalently bound AB dimer and the dimer in the environment of other AB molecules, imitating with the latter a densely packed SAM. Specifically, we studied three models of increasing sophistication: (i) an AB monomer as a reference, (ii) an isolated QM dimer (Fig. 1 (a)) and (iii) the QM dimer surrounded by ten frozen MM AB monomers,

interacting with the QM central dimer through classical pairwise atomic vdW interactions only (Fig. 1 (b–d)). We will refer to the latter model as "SAM" or the vdW-constrained dimer in what follows.

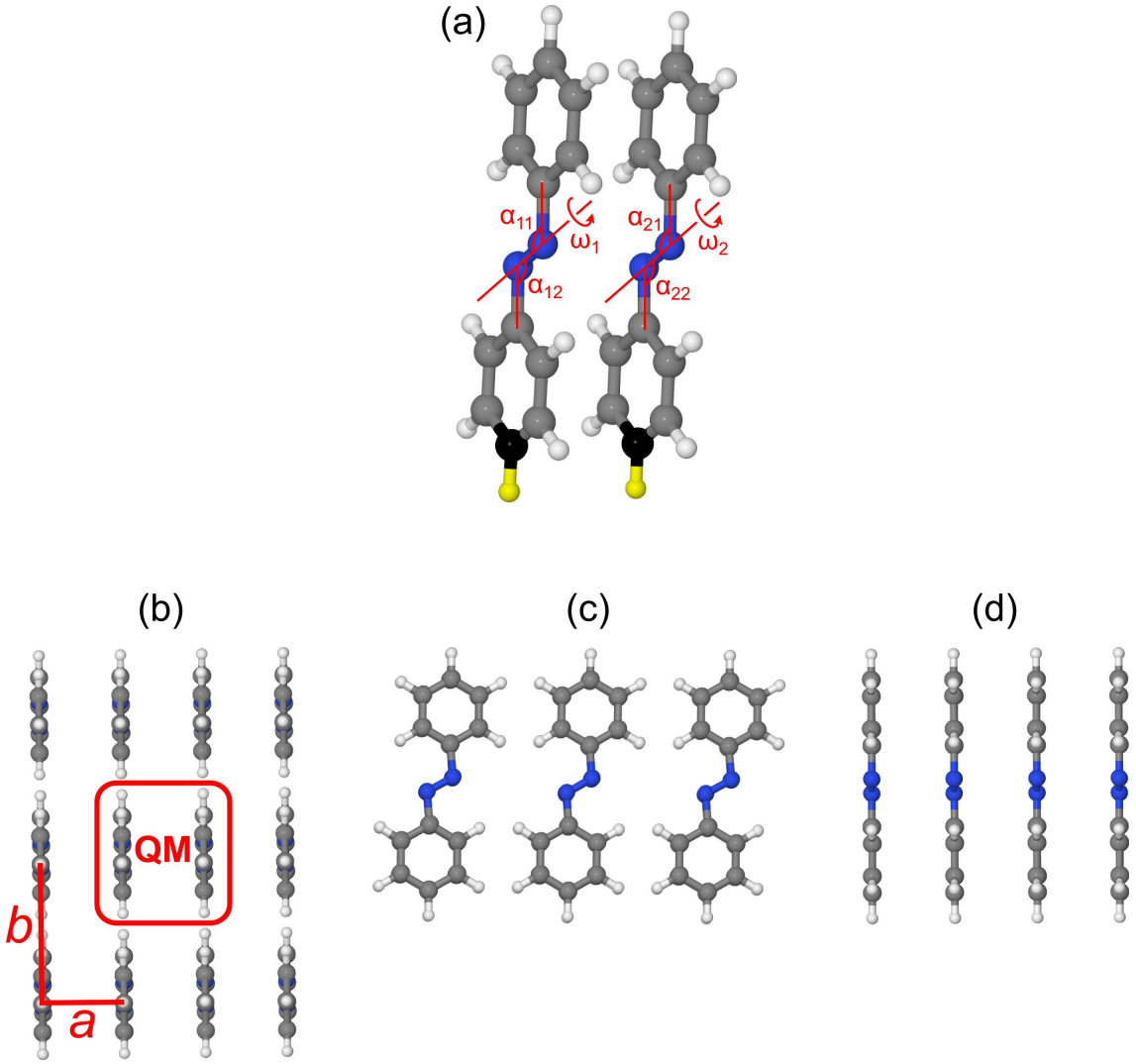


Figure 1: (a) The AB dimer along with angles relevant for isomerization, namely CNN angles ($\alpha$) and CNNC dihedrals ($\omega$). The two molecules are placed exactly side by side as shown, with molecular planes on top of each other and a distance between the molecular planes of 3.5 Å. Black (carbon) and yellow (hydrogen) balls represent the atoms which were fixed during dynamics. (b–d) Different views of the AB "SAM" model: (b) top view, separation parameters $a = 3.5$ Å and $b = 6.0$ Å, the QM part (the central dimer) is marked by the red frame; (c) first side view; (d) second side view.

Here, the initial geometry of a *trans*-AB molecule was determined at the B3LYP[19,20]/6-31G*[21,22] level of theory. Note that the "SAM" model is highly idealized, with upright (rather

than tilted) molecules arranged in a rectangular unit cell, with lattice parameters $a = 3.5$ Å and $b = 6.0$ Å providing a high area density of $\sim$5 molecules per nm$^2$. For comparison, the densely packed molecular arrangement of Ref. 1 was $\sim$4.2 molecules per nm$^2$; in Ref. 23, a critical grafting density beyond which switching in AB-containing SAMs is suppressed of about 2.5 molecules per nm$^2$ has been given. Further, the surface is only indirectly included in our proof-of-principle model, through a specific choice of lattice parameters and the fact that the two lowest carbon and hydrogen atoms of the lower phenyl ring of each molecule of the QM dimer (for both models (ii) and (iii)) are kept fixed during the MD runs, *cf.* Fig. 1. As such, model (i) represents a totally unconstrained switch, model (ii) an electronically coupled dimer with slight steric hindrance, and model (iii) an electronically coupled dimer with strong steric constraints imposed by an environment. We should stress that in our third model ("SAM") the MM perimeter molecules are frozen during dynamics allowing for regular molecular arrangement, which provides, in turn, the needed steric hindrance. However, with this we omit the vibrational energy transfer from the QM part to the MM one. These two factors are expected to affect a quantum yield in different directions.

Singlet excited states, gradients and nonadiabatic couplings required in the QM treatment and surface hopping dynamics were calculated "on the fly" by means of the semiempirical reparameterized AM1/FOMO-CI method.[15,24–27] For all models, the same active space and CI procedure as previously employed for bisazobenzenes was used.[16] Out of calculated excited states, the energetically lowest 14 singlet excited states (plus the ground state) were used for surface hopping dynamics. Note that these states include the singlet combinations of the two monomer triplets. However, we did not consider overall triplets and intersystem crossing transitions because the azobenzene $T_1$ and $S_1$ states are far enough in energy and share the same $n\pi^*$ configuration, so they are expected to interact weakly by spin–orbit coupling, according to El-Sayed rules. For the "SAM" QM/MM model, vdW interactions with the surrounding AB molecules were described by the MM3-2000 force field.[28,29] Further

details on models and methods are presented in the SI.

First, we calculated vertical absorption spectra of the *trans* monomer and dimer (at $T = 0$ K) using various first-principles (DFT and wavefunction-based) methods to judge on the performance of AM1/FOMO-CI for the systems under study. A detailed discussion of spectra and method dependencies is presented in the SI. Briefly, semiempirical (AM1/FOMO-CI) spectra are energetically close (in terms of a location of the $\pi\pi^*$ absorption band) to time-dependent Hartree-Fock (TD-HF) (see, *e.g.*, Refs. 30, 31) ones, showing a blue shift with respect to other methods and to an available experimental gas-phase result[32] (Fig. S2, Tabs. S1 and S2). The blue shift relative to modern range-separated functionals (*e.g.*, M11[33] or $\omega$B97[34]) or SCS-CC2[35] is rather moderate, $\sim$0.1–0.25 eV. Moreover, AM1/FOMO-CI shows the presence of several doubly excited states, as verified also by the so-called DFT/MRCI method[36] which accounts for multiple-excitations as AM1/FOMO-CI. We also find, when going from monomer to the dimer, an expected blue shift (except for DFT/MRCI, which is not suitable for the dimers[37]) and enhancement of the $\pi\pi^*$ signal. The blue shift is around 0.1–0.2 eV for most methods (Figs. S2 and S3). It is due to the fact that the $\pi\pi^*$ transition is split by exciton coupling into a red-shifted dark and a blue-shifted bright state, the so-called *Davydov (or exciton) splitting.*[38,39] With the present short intermolecular distances and ideal upright orientation the exciton splitting $\Delta\mathcal{E}_{exciton}$ between the two states is quite large and in the order of 0.6–0.7 eV, only moderately method-dependent (see Fig. S3). From these findings we conclude that the AM1/FOMO-CI method is sufficiently accurate to correctly account for excited-state properties of coupled AB dimers. The description of photoisomerization pathways and conical intersections obtained at the AM1/FOMO-CI level for the azobenzene is presented in Ref. 27.

In a second step, initial coordinates and velocities for subsequent photodynamics were sampled from Brownian trajectories[40] on the ground state potential energy surface (PES),

using the AM1/FOMO-CI method. Brownian dynamics were run once for each model (i)–(iii) for 10 ps at a temperature of 300 K. Initial structures for photoexcitation were selected after 1 ps. When computing vertical excitation energies (wavelengths) and transition dipole moments (and corresponding oscillator strengths) for each geometry along the Brownian trajectory and subsequently broadening the stick spectra by Gaussian functions (see SI for details), we can estimate thermally broadened absorption spectra for the *trans*-AB species. The resulting spectra, averaged along the Brownian trajectories are presented in Fig. 2. Specifically, $\pi\pi^*$ and $n\pi^*$ bands are shown in plots (a) and (b), respectively, for all three models (*i.e.*, monomer, isolated dimer, and "SAM").

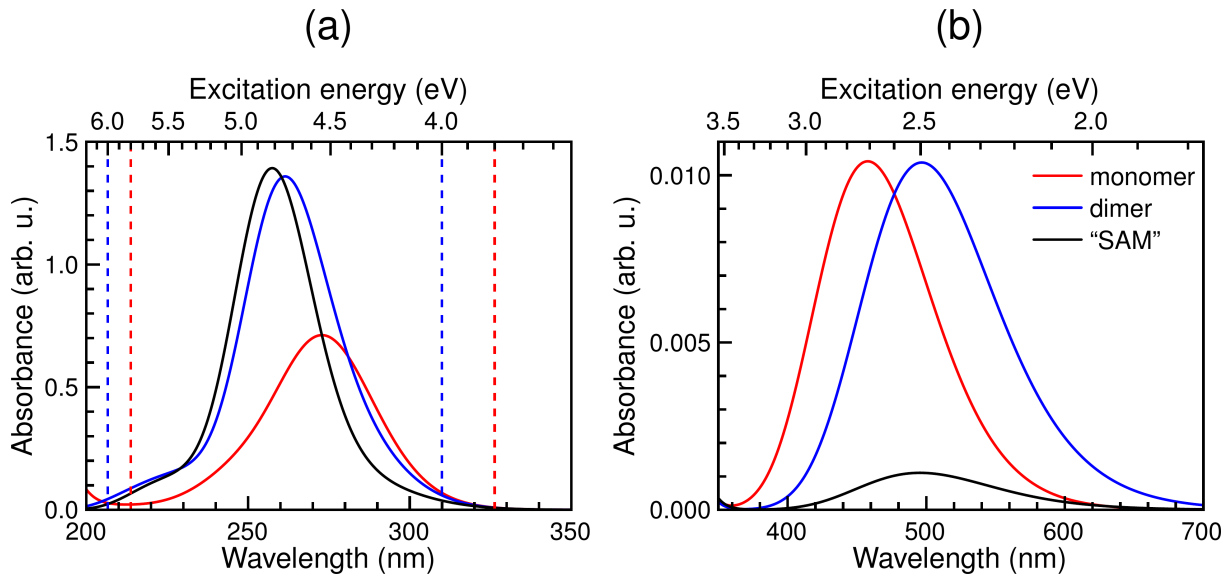


Figure 2: Averaged (along ground-state Brownian trajectories) broadened vertical absorption spectra for monomer (red solid lines), isolated dimer (blue), and "SAM" (black): (a) $\pi\pi^*$ band, (b) $n\pi^*$ band . Dashed lines in (a) show the boundaries of the energy windows to select initial PESs for the photodynamics: red for the monomer and blue for the isolated dimer and "SAM". For details on the broadening procedure see SI.

From Fig. 2 (a) we note also here the mentioned blue shift (by ∼0.2 eV) and intensity enhancement (by a factor of about two) of the lowest bright $\pi\pi^*$ transition upon dimerization, compared to the monomer, in agreement with the Davydov model. The effect of constraining the dimer by a SAM-like environment on the $\pi\pi^*$ band is small. Due to thermal distortions the $n\pi^*$ transitions of the *trans* isomers become partially allowed (Fig. 2 (b)). Note that the

spectral features of the $n\pi^*$ band behave differently than the $\pi\pi^*$ band as far as effects of dimerization and steric constraints are concerned (see SI for the discussion of the $n\pi^*$ band behaviour). In what follows, however, we focus on excitations into the $\pi\pi^*$ band which is much more intense than the $n\pi^*$ one.

In a third step, we modeled the post-excitation dynamics (which may lead to isomerization) of our three systems, after optical excitations of the thermalized *trans* species into the $\pi\pi^*$ band. The corresponding energy windows selected for these excitations are shown with dashed lines in Fig. 2 (a). For all the models the size of the windows is 2 eV — we assigned a window of [3.8,5.8] eV for the monomer and [4.0,6.0] eV for the isolated dimer and "SAM". Selecting the initial electronic states was done as described elsewhere[40] based on the magnitudes of transition dipole moments from ground to the excited states which fall into the energy window. Moreover, we ensured that each single geometry selected from the Brownian trajectory was used only once as an initial geometry for photodynamics.

Next, multiple surface hopping trajectories, starting at the selected $\pi\pi^*$ states were launched. Examples of different kinds of trajectories, represented with CNN angles ($\alpha$) and CNNC dihedrals ($\omega$), are depicted in Fig. 3 (see also Fig. 1 (a) for definition of angles). Fig. 3 gives also information on which singlet potential energy surface the trajectory resides at a given moment. We find "reactive", "unreactive", and "undetermined" trajectories. The reactive trajectories shown in the left column of Fig. 3, *i.e.*, those trajectories for which *trans* $\rightarrow$ *cis* isomerization took place, demonstrate after some time ($\lesssim$ 1 ps for the trajectories of Fig. 3) the change of the $\omega$-value from $\sim$180° (*trans* isomer) to $\sim$0° (*cis* isomer). Switching often occurs around the time when a $n\pi^* \rightarrow$ ground state transition happens. The mechanism of the isomerization is complex and involves the increase of $\alpha$ angles with subsequent rearrangement of the CNNC moiety to the *cis* form.

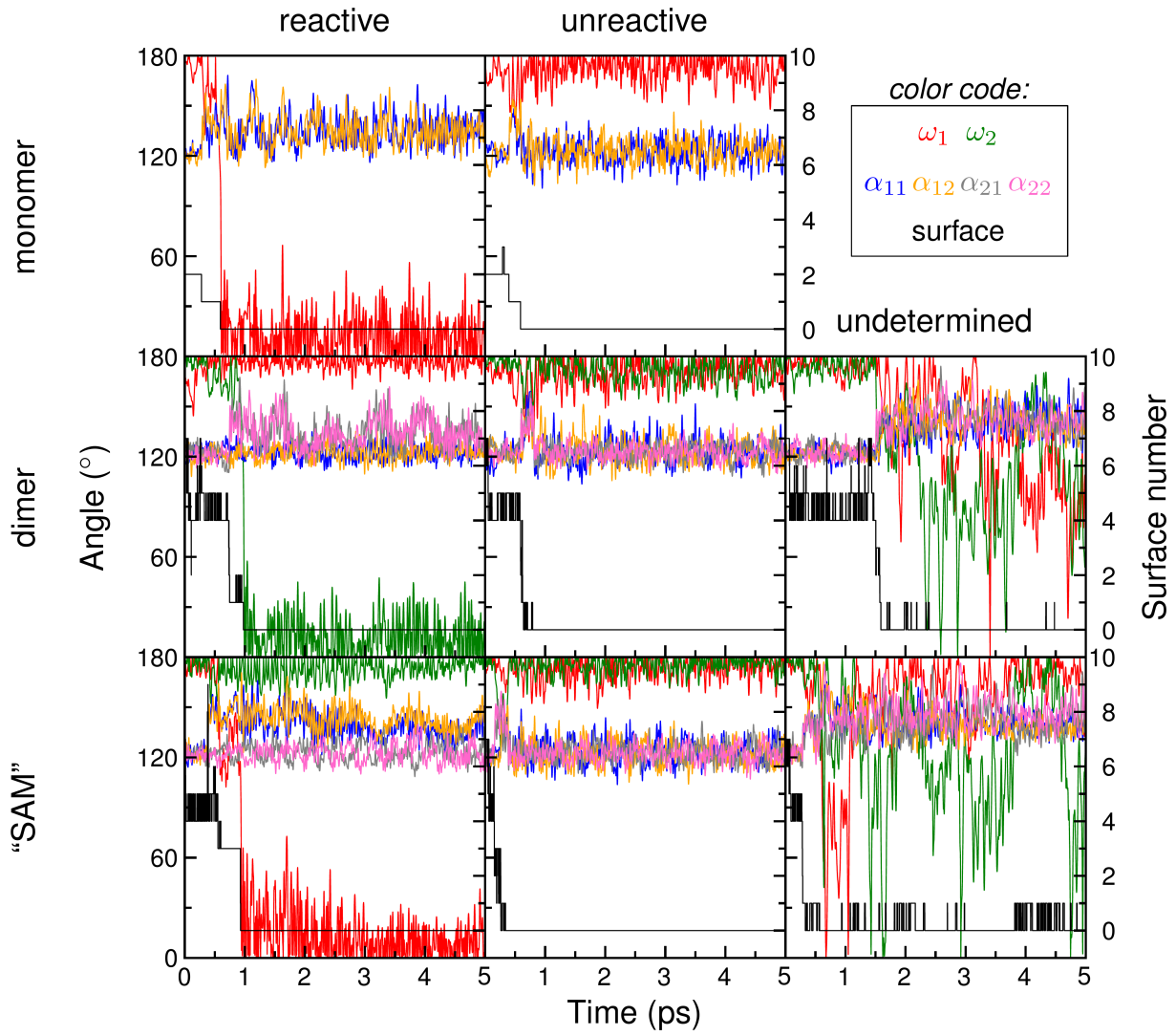


Figure 3: Selected nonadiabatic trajectories for the three models under study: Shown are dihedral CNNC ($\omega_1$, $\omega_2$) and CNN ($\alpha_{11}$, $\alpha_{12}$, $\alpha_{21}$, $\alpha_{22}$) angles (*cf.* Fig. 1) (left scale) as well as PES numbers (right scale, the number $n$ denoting state $S_n$) as a function of time. The left column represents reactive trajectories, middle — unreactive, and right — undetermined ones.

Note that in the dimeric models only one molecule is switched while the other stays in the *trans* form (with $\omega$ about 180°). This is true for all reactive trajectories on a timescale of 5 ps. The unreactive trajectories, *i.e.*, the trajectories for which excited *trans* models relaxed without reaching the *cis* isomer are shown in the middle column of Fig. 3. For the dimeric models, in contrast to the monomer, some trajectories (Fig. 3, right column) demonstrate large-amplitude changes of dihedral angles during dynamics, and can be referred

to as undetermined. On longer timescales, when including vibrational relaxation, these trajectories would eventually become reactive or unreactive, respectively.

Counting reactive trajectories one can define the *trans* $\rightarrow$ *cis* quantum yield $\Phi$ as the ratio of the number of reactive trajectories, $N_{react}$, to the total number of reactive and unreactive trajectories, $N_{tot}$, $\Phi = N_{react}/N_{tot}$ (undetermined trajectories were not included in the analysis). The quantum yields along with bootstrap estimate of the standard error of the mean[41] $\Delta\Phi = \sqrt{\Phi(1-\Phi)/N_{tot}}$ are presented in Tab. 1.

**Table 1: Quantum yield ($\Phi$) of the *trans* $\rightarrow$ *cis* isomerization after $\pi\pi^*$ excitation and lifetimes ($\tau$) of excited $\pi\pi^*$ and $n\pi^*$ states for the three models under study**

| Model | $N^a_{tot}$ | $N^b_{undetermined}$ | $\Phi^c$ | $\tau_{\pi\pi^*}$ (fs) | $\tau_{n\pi^*}$ (fs) |
|---|---|---|---|---|---|
| Monomer | 73 | 0 | $0.21 \pm 0.05$ | 308 | 225 |
| Dimer | 70 | 16 | $0.19 \pm 0.05$ | 1471 | 260 |
| "SAM" | 103 | 149 | $0.11 \pm 0.03$ | 500 | 552 |

[a] $N_{tot}$ is the total number of reacive and unreactive trajectories.
[b] $N_{undetermined}$ is the number of undetermined trajectories (*cf.* Fig. 3, right column).
[c] The standard error for yields $\Delta\Phi$ is determined as described in the text.

We first of all note that the quantum yield for the monomer is 0.21.[42] This value agrees fairly well with the quantum yield of 0.25 found recently[6] using corrected PESs[27] and an energy based decoherence correction (EDC)[18] (this latter correction was also applied in our calculations in the present work) for surface hopping. The quantum yield for the isolated dimer is very similar, 0.19. Thus, the switching probability for the free dimer is approximately as high as for the monomer. When restricting the dimer sterically within the "SAM" model, the quantum yield is greatly reduced, to 0.11. Since in the isolated dimer electronic coupling is present but steric hindrance is small while in the "SAM" dimer steric hindrance is large, we conclude that for the present model system at least *steric hindrance appears as the dominating effect which suppresses the switching probability of densely packed monolayers of AB molecules.*

Further, we compute state populations — fractions of trajectories being at a given time in a certain electronic state. For this analysis we considered all trajectories, reactive, unreactive, and undetermined, for each of the studied models. We combined $n\pi^*$ excited states in one group and $\pi\pi^*$ excited states in another one. Specifically, for the monomer $n\pi^*$ corresponds to $S_1$, and the $\pi\pi^*$ group to $S_2$ and higher. For the isolated dimer and "SAM", the $n\pi^*$ group includes three states $S_1$ to $S_3$, whereas $\pi\pi^*$ includes $S_4$ and higher states. The populations were fitted by using a two-step irreversible kinetics model (Fig. 4 (a)), giving lifetimes $\tau_{\pi\pi^*}$ and $\tau_{n\pi^*}$ of the respective excited state manifolds:[16]

$$P_{\pi\pi^*} = e^{-t/\tau_{\pi\pi^*}} \tag{1}$$

$$P_{n\pi^*} = \frac{\tau_{n\pi^*}}{\tau_{n\pi^*} - \tau_{\pi\pi^*}}(e^{-t/\tau_{n\pi^*}} - e^{-t/\tau_{\pi\pi^*}}) \tag{2}$$

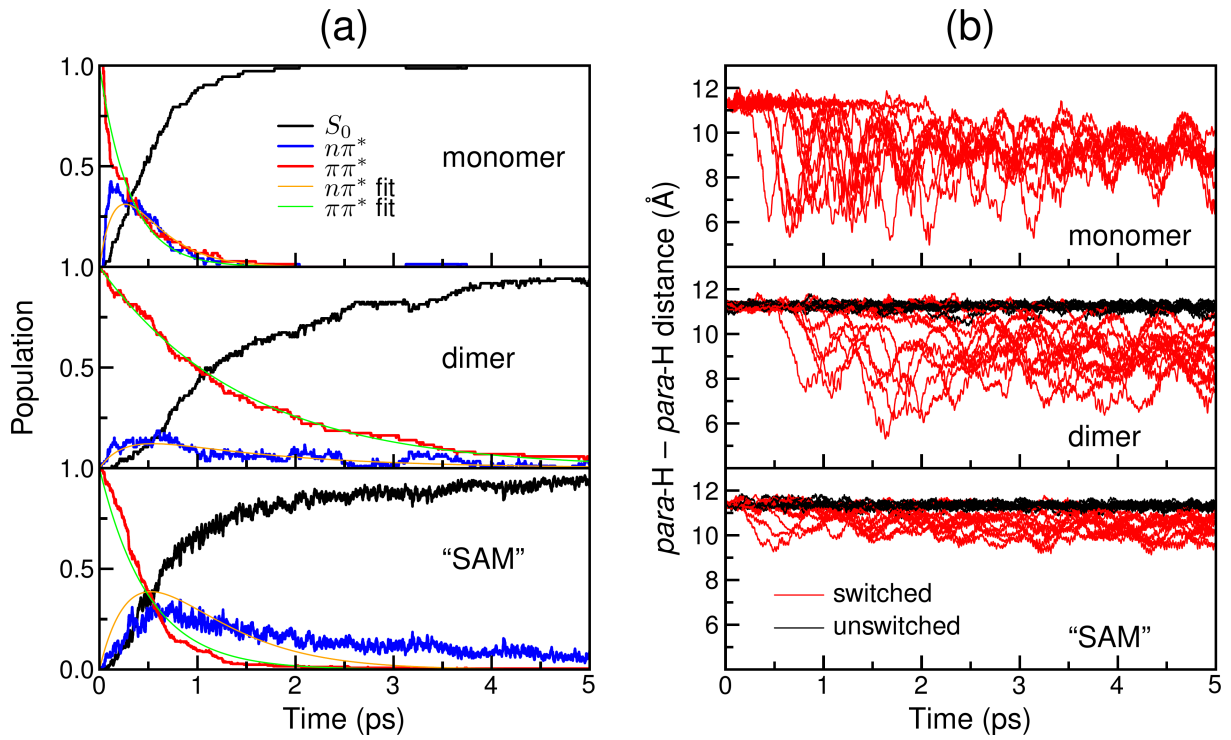


Figure 4: (a) Time evolution of populations (fractions of trajectories) for the ground state ($S_0$), $n\pi^*$ and $\pi\pi^*$ states. (b) Time evolution of the end-to-end distance (between hydrogen atoms in *para*-positions of the phenyl rings) for the reactive trajectories.

Inspection of the lifetimes as tabulated in Tab. 1 indicates that the lifetime of the $\pi\pi^*$ states is almost five times larger for the isolated dimer than for the monomer, increasing from about 300 to close to 1500 fs. As a result of the excitonic coupling between $\pi\pi^*$ states, in the dimer the higher state of the Davydov split pair is populated. The energy gap between this state and the $n\pi^*$ ones is larger than in the monomer and this may explain its slower decay. Interestingly, the long lifetime for the isolated dimer is considerably reduced, by a factor of three, for the "SAM" dimer, showing that the vdW constraint leads to a faster decay of the $\pi\pi^*$ states, to $n\pi^*$. We have verified that the torsion of the CN bonds (NNCC dihedral angles), while the trajectories evolve in the $\pi\pi^*$ states, is more free in the dimer than in the "SAM" (Fig. S6). The same is true, to a lesser extent, for the NN bond torsion (CNNC dihedral). This kind of geometrical relaxation increases the energy gap with the $n\pi^*$ states (see Fig. 1 and Tab. 5 of Ref. 6). In fact we find in the average larger energy gaps in the dimer than in the "SAM" (Fig. S7), which explains the difference in the $\pi\pi^*$ lifetime. The lifetime of the $n\pi^*$ states, in comparison to the monomer, is somewhat larger for the isolated dimer and greatly increased for the "SAM", due to population of the $n\pi^*$ states from the ground state during all 5 ps in the case of undetermined trajectories. Note that the excited state lifetimes are not directly related to switching yields.

Finally, we compared the change in the end-to-end distance of the AB molecule (molecular length) upon the *trans* $\rightarrow$ *cis* isomerization. To do so we tracked the distance between hydrogen atoms in *para*-positions of the phenyl rings of AB, for reactive trajectories only (Fig. 4 (b)). We find that the *cis* isomer length spans a broader range of distances in the case of the monomer and the free dimer than for the "SAM" dimer. In other words, the vdW-constraint keeps the molecules in a more open form (larger end-to-end distance) after the *trans* $\rightarrow$ *cis* isomerization. As another consequence of the steric confinement in addition to altered excited state lifetimes and switching probabilities, therefore, also the geometry of the switched molecules differs: In the confined dimer, they stay in a *trans*-

typical elongated form after switching, however, with a dihedral angle characteristic for the *cis* form. In the unconstrained dimer, both characteristics (molecular length and dihedral) change substantially.

In conclusion, we performed nonadiabatic molecular dynamics simulations for free and vdW-constrained ("SAM") AB dimers. We treated both dimer molecules using the AM1/FOMO-CI method, thus accounting for the change in electronic structure upon dimerization. Importantly, we found (i) a very similar *trans* $\rightarrow$ *cis* quantum yield (after $\pi\pi^*$ excitation) for the free dimer ($\Phi = 0.19 \pm 0.05$) in comparison to the monomeric reference ($\Phi = 0.21 \pm 0.05$), and (ii) pronounced decrease of the quantum yield for the "SAM" ($\Phi = 0.11 \pm 0.03$). We conclude that in the present model at least (which has both strong electronic coupling and large steric hindrance), steric effects are the main reason why switching is suppressed in densely packed monolayers of AB molecules on surfaces. We further found that the lifetimes of the excited states for the dimer models are increased in comparison to the monomer. The end-to-end distance of the *cis* isomer, formed after photoisomerization, is on average larger for the "SAM" model, suggesting that steric confinement can also lead to different product geometries.

Of course, the present models should be refined in the future. In particular, enlargement of the QM part, inclusion of motion for the MM environment, inclusion of the substrate and, finally, a systematic study of effects of the packing density are worthwhile directions to go.

***Acknowledgements.*** This research was done in the framework of the IMPRS on Multiscale Bio-Systems. We thank Dr. G. Floß for most valuable discussions. We are grateful to Prof. W. Thiel for computational time for the DFT/MRCI calculations.

## Supporting Information Available

Details on models and dynamical calculations; absorption spectra, spectral shift, and exciton splitting; CN and NN bond torsions during Brownian and photodynamics. This material is available free of charge via the Internet at `http://pubs.acs.org/`.

## Notes and References


(1) Gahl, C.; Schmidt, R.; Brete, D.; McNellis, E. R.; Freyer, W.; Carley, R.; Reuter, K.; Weinelt, M. Structure and Excitonic Coupling in Self-Assembled Monolayers of Azobenzene-Functionalized Alkanethiols. *J. Am. Chem. Soc.* **2010**, *132*, 1831–1838.

(2) Valley, D. T.; Onstott, M.; Malyk, S.; Benderskii, A. V. Steric Hindrance of Photoswitching in Self-Assembled Monolayers of Azobenzene and Alkane Thiols. *Langmuir* **2013**, *29*, 11623–11631.

(3) Ciminelli, C.; Granucci, G.; Persico, M. The Photoisomerization Mechanism of Azobenzene: A Semiclassical Simulation of Nonadiabatic Dynamics. *Chem. - Eur. J.* **2004**, *10*, 2327–2341.

(4) Toniolo, A.; Ciminelli, C.; Persico, M.; Martínez, T. J. Simulation of the Photodynamics of Azobenzene on Its First Excited State: Comparison of Full Multiple Spawning and Surface Hopping Treatments. *J. Chem. Phys.* **2005**, *123*, 234308.

(5) Cusati, T.; Granucci, G.; Persico, M. Photodynamics and Time-Resolved Fluorescence of Azobenzene in Solution: A Mixed Quantum-Classical Simulation. *J. Am. Chem. Soc.* **2011**, *133*, 5109–5123.

(6) Cantatore, V.; Granucci, G.; Persico, M. Simulation of the $\pi \rightarrow \pi^*$ Photodynamics of Azobenzene: Decoherence and Solvent Effects. *Comput. Theor. Chem.* **2014**, *1040–1041*, 126–135.

(7) Fabiano, E.; Groenhof, G.; Thiel, W. Approximate Switching Algorithms for Trajectory Surface Hopping. *Chem. Phys.* **2008**, *351*, 111–116.

(8) Weingart, O.; Lan, Z.; Koslowski, A.; Thiel, W. Chiral Pathways and Periodic Decay in *cis*-Azobenzene Photodynamics. *J. Phys. Chem. Lett.* **2011**, *2*, 1506–1509.

(9) Gámez, J. A.; Weingart, O.; Koslowski, A.; Thiel, W. Cooperating Dinitrogen and Phenyl Rotations in *trans*-Azobenzene Photoisomerization. *J. Chem. Theory Comput.* **2012**, *8*, 2352–2358.

(10) Böckmann, M.; Doltsinis, N. L.; Marx, D. Azobenzene Photoswitches in Bulk Materials. *Phys. Rev. E* **2008**, *78*, 036101.

(11) Böckmann, M.; Doltsinis, N. L.; Marx, D. Nonadiabatic Hybrid Quantum and Molecular Mechanic Simulations of Azobenzene Photoswitching in Bulk Liquid Environment. *J. Phys. Chem. A* **2010**, *114*, 745–754.

(12) Pederzoli, M.; Pittner, J.; Barbatti, M.; Lischka, H. Nonadiabatic Molecular Dynamics Study of the *cis–trans* Photoisomerization of Azobenzene Excited to the $S_1$ State. *J. Phys. Chem. A* **2011**, *115*, 11136–11143.

(13) Floß, G.; Granucci, G.; Saalfrank, P. Surface Hopping Dynamics of Direct *trans* $\rightarrow$ *cis* Photoswitching of an Azobenzene Derivative in Constrained Adsorbate Geometries. *J. Chem. Phys.* **2012**, *137*, 234701.

(14) Benassi, E.; Granucci, G.; Persico, M.; Corni, S. Can Azobenzene Photoisomerize When Chemisorbed on a Gold Surface? An Analysis of Steric Effects Based on Nonadiabatic Dynamics Simulations. *J. Phys. Chem. C* **2015**, *119*, 5962–5974.

(15) Ciminelli, C.; Granucci, G.; Persico, M. Are Azobenzenophanes Rotation-Restricted? *J. Chem. Phys.* **2005**, *123*, 174317.

(16) Floß G.; Saalfrank, P. The Photoinduced $E \rightarrow Z$ Isomerization of Bisazobenzenes: A Surface Hopping Molecular Dynamics Study. *J. Phys. Chem. A* **2015**, *119*, 5026–5037.

(17) Tully, J. C. Molecular Dynamics with Electronic Transitions. *J. Chem. Phys.* **1990**, *93*, 1061–1071.

(18) Granucci, G.; Persico, M. Critical Appraisal of the Fewest switches Algorithm for Surface Hopping. *J. Chem. Phys.* **2007**, *126*, 134114.

(19) Becke, A. D. Density-Functional Thermochemistry. III. The Role of Exact Exchange. *J. Chem. Phys.* **1993**, *98*, 5648–5652.

(20) Stephens, P. J.; Devlin, F. J.; Chabalowski, C. F.; Frisch, M. J. Ab Initio Calculation of Vibrational Absorption and Circular Dichroism Spectra Using Density Functional Force Fields. *J. Phys. Chem.* **1994**, *98*, 11623–11627.

(21) Hehre, W. J.; Ditchfield, R.; Pople, J. A. Self-Consistent Molecular Orbital Methods. XII. Further Extensions of Gaussian-Type Basis Sets for Use in Molecular Orbital Studies of Organic Molecules. *J. Chem. Phys.* **1972**, *56*, 2257–2261.

(22) Hariharan, P.; Pople, J. The Influence of Polarization Functions on Molecular Orbital Hydrogenation Energies. *Theor. Chim. Acta* **1973**, *28*, 213–222.

(23) Klajn, R. Immobilized Azobenzenes for the Construction of Photoresponsive Materials. *Pure Appl. Chem.* **2010**, *82*, 2247–2279.

(24) Dewar, M. J. S.; Zoebisch, E. G.; Healy, E. F.; Stewart, J. J. P. Development and Use of Quantum Mechanical Molecular Models. 76. AM1: A New General Purpose Quantum Mechanical Molecular Model. *J. Am. Chem. Soc.* **1985**, *107*, 3902–3909.

(25) Granucci, G.; Toniolo, A. Molecular Gradients for Semiempirical {CI} Wavefunctions with Floating Occupation Molecular Orbitals. *Chem. Phys. Lett.* **2000**, *325*, 79–85.

(26) Granucci, G.; Persico, M.; Toniolo, A. Direct Semiclassical Simulation of Photochemical Processes with Semiempirical Wave Functions. *J. Chem. Phys.* **2001**, *114*, 10608–10615.

(27) Cusati, T.; Granucci, G.; Martínez-Núñez, E.; Martini, F.; Persico, M.; Vázquez, S. Semiempirical Hamiltonian for Simulation of Azobenzene Photochemistry. *J. Phys. Chem. A* **2012**, *116*, 98–110.

(28) Lii, J. H.; Allinger, N. L. Molecular Mechanics. The MM3 Force Field for Hydrocarbons. 3. The van der Waals' Potentials and Crystal Data for Aliphatic and Aromatic Hydrocarbons. *J. Am. Chem. Soc.* **1989**, *111*, 8576–8582.

(29) Tai, J. C.; Yang, L.; Allinger, N. L. Molecular Mechanics (MM3). Calculations on Nitrogen-Containing Aromatic Heterocycles. *J. Am. Chem. Soc.* **1993**, *115*, 11906–11917.

(30) Dreuw, A.; Head-Gordon, M. Single-Reference Ab Initio Methods for the Calculation of Excited States of Large Molecules. *Chem. Rev.* **2005**, *105*, 4009–4037.

(31) Casida, M.; Huix-Rotllant, M. Progress in Time-Dependent Density-Functional Theory. *Annu. Rev. Phys. Chem.* **2012**, *63*, 287–323.

(32) Andersson, J.-Å.; Petterson, R.; Tegnér, L. Flash Photolysis Experiments in the Vapour Phase at Elevated Temperatures I: Spectra of Azobenzene and the Kinetics of Its Thermal *cis-trans* Isomerization. *J. Photochem.* **1982**, *20*, 17–32.

(33) Peverati, R.; Truhlar, D. G. Improving the Accuracy of Hybrid Meta-GGA Density Functionals by Range Separation. *J. Phys. Chem. Lett.* **2011**, *2*, 2810–2817.

(34) Chai, J.-D.; Head-Gordon, M. Systematic Optimization of Long-Range Corrected Hybrid Density Functionals. *J. Chem. Phys.* **2008**, *128*, 084106.

(35) Hellweg, A.; Grün, S. A.; Hättig, C. Benchmarking the Performance of Spin-Component Scaled CC2 in Ground and Electronically Excited States. *Phys. Chem. Chem. Phys.* **2008**, *10*, 4119–4127.

(36) Grimme, S.; Waletzke, M. A Combination of Kohn–Sham Density Functional Theory and Multi-Reference Configuration Interaction Methods. *J. Chem. Phys.* **1999**, *111*, 5645–5655.

(37) Lyskov, I.; Kleinschmidt, M.; Marian, C. M. Redesign of the DFT/MRCI Hamiltonian. *J. Chem. Phys.* **2016**, *144*, 034104.

(38) Davydov, A. S. The Theory of Molecular Excitons. *Soviet Physics Uspekhi* **1964**, *7*, 145–178.

(39) Titov, E.; Saalfrank, P. Exciton Splitting of Adsorbed and Free 4-Nitroazobenzene Dimers: A Quantum Chemical Study. *J. Phys. Chem. A* **2016**, *120*, 3055–3070.

(40) Creatini, L.; Cusati, T.; Granucci, G.; Persico, M. Photodynamics of Azobenzene in a Hindering Environment. *Chem. Phys.* **2008**, *347*, 492–502.

(41) Efron, B.; Tibshirani, R. Bootstrap Methods for Standard Errors, Confidence Intervals, and Other Measures of Statistical Accuracy. *Statist. Sci.* **1986**, *1*, 54–75.

(42) Note that in Ref. 16 the quantum yield of $0.12 \pm 0.03$ was reported for the AB monomer, obtained using the same method as we employed here. The discrepancy between the values can be explained as follows. Here we observed that some trajectories, after the molecule switched to the *cis* form and stayed in this form for hundreds of femtoseconds, exhibit the back isomerization to the *trans* form (being in the electronic ground state). All these back isomerizations happen before 3 ps — the time used in Ref. 16 as the landmark time to stop trajectories based on certain criteria (see section C.2 of Ref. 16 for further details). Excluding such trajectories from the reactive set in the present work will give a yield of 0.12. However, we believe that these back isomerizations are nonphysical and caused by the use of the AM1 method without an added potential (see Ref. 27).

# Supporting Information for: "Dynamics of Azobenzene Dimer Photoisomerization: Electronic and Steric Effects"

Evgenii Titov,[†] Giovanni Granucci,[‡] Jan Philipp Götze,[†] Maurizio Persico,[‡] and Peter Saalfrank[*,†]

*Theoretical Chemistry, Institute of Chemistry, University of Potsdam, Karl-Liebknecht-Str. 24-25, 14476 Potsdam, Germany, and Department of Chemistry and Industrial Chemistry, University of Pisa, via Moruzzi 13, 56124 Pisa, Italy*

E-mail: peter.saalfrank@uni-potsdam.de

[*]To whom correspondence should be addressed

[†]Theoretical Chemistry, Institute of Chemistry, University of Potsdam, Karl-Liebknecht-Str. 24-25, 14476 Potsdam, Germany

[‡]Department of Chemistry and Industrial Chemistry, University of Pisa, via Moruzzi 13, 56124 Pisa, Italy

## Details on models and dynamical calculations

The geometry of the *trans*-azobenzene (AB) monomer in the electronic ground state was optimized at the B3LYP[S1,S2]/6-31G*[S3,S4] level of theory using Gaussian 09 (Revision D.01).[S5] The minimum nature of the obtained structure was proven by vibrational frequency analysis, which yielded only real frequencies. The geometry of the monomer was found to be planar. This structure was used as a starting geometry for model (i) of the main text (monomer), but also for the dimer models (ii) (isolated dimer) and (iii) ("SAM" model).

The dimer model (ii) was constructed by applying a translation of 3.5 Å to all atoms of the optimized monomer in the direction perpendicular to the molecular plane. The "SAM" model (iii) was constructed by further translating AB monomers as shown in Fig. 1 (b–d) of the main text. Note that the simple translation was chosen for the dimer and "SAM" construction (instead of, *e.g.*, optimization of the geometry with DFT plus a dispersion correction) to have the same intermolecular separation and molecular arrangement for the free dimer and the "SAM", which can also be easily varied to study, *e.g.*, packing density effects. For both the free and the vdW-constrained models, the four bottom atoms of the QM dimer, two carbons and two hydrogens, were frozen during the dynamics to keep two AB molecules together.

The potential energy surfaces (PESs), gradients and nonadiabatic couplings were calculated "on the fly" by means of semiempirical (reparameterized for the single AB molecule AM1[S6,S7]) configuration interaction (CI), employing SCF molecular orbitals (MO) with floating occupation (FO) numbers[S8–S10] (abbreviated as AM1/FOMO-CI) by using the development version of the MOPAC 2002 program.[S11] The active space (for all models) contained 22 electrons in 21 orbitals. In the CI, all single excitations within active space plus multiple excitations within complete active (sub)space (CAS) of 8 electrons in 6 orbitals were included. This method, denoted as AM1/FOMO-CI/(22,21)/(8,6), was used previously

for the bisazobenzenes.[S12] Note that we did not use the added potential and state-specific corrections for the PESs, developed previously for the single AB molecule.[S7] The molecular orbitals comprising the CAS are presented in Fig. S1. It is seen that the six frontier orbitals of the dimer correspond to the HOMO−1 ($\pi$), HOMO ($n$), and LUMO ($\pi^*$) of the monomer.

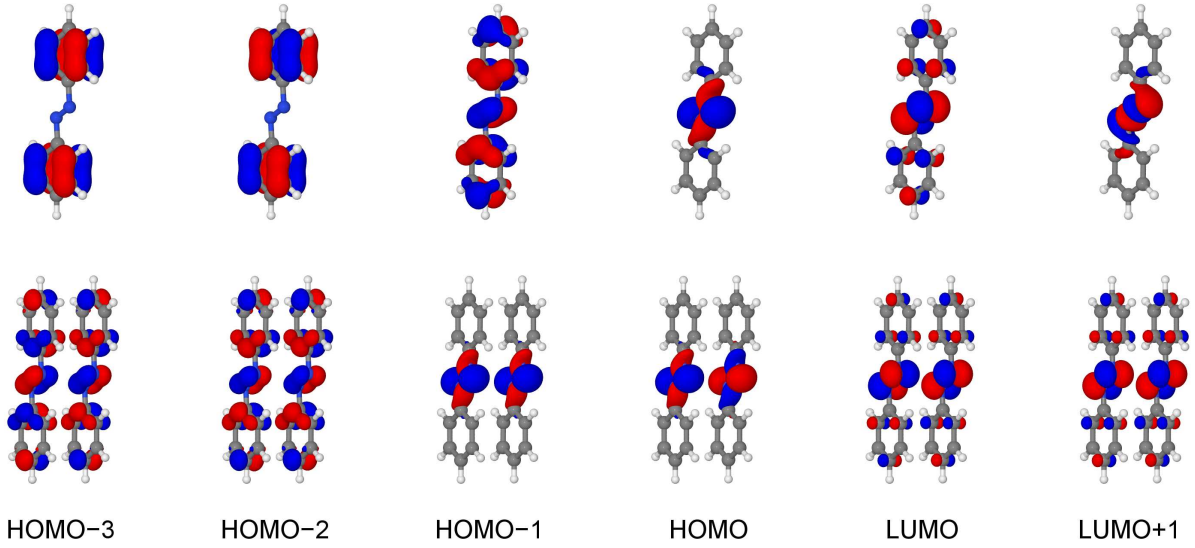


Figure S1: Molecular orbitals comprising the complete active (sub)space (CAS).

The vdW interactions for the "SAM" model were treated by means of the MM3-2000 force field[S13,S14] with the help of the TINKER package.[S15] The MM molecules were kept fixed during the simulation.

The first 15 singlet states (ground and 14 excited) were used for the surface hopping dynamics, for all models.

## Absorption spectra, spectral shift, and exciton splitting

We calculated vertical absorption spectra of the *trans* monomer and the *trans–trans* dimer using various methods to judge on the performance of AM1/FOMO-CI approach used for the dynamics afterwards. Altogether 18 methods were used: AM1/FOMO-CI/(22,21)/(8,6); DFT/MRCI[S16]/def2-SVP;[S17,S18] TD-HF (see, *e.g.*, Refs. S19, S20)/6-

31G*; TD-DFT (see, *e.g.*, Ref S21)/6-31G* with the following functionals: BHandHLYP (Gaussian 09 implementation, for "half-and-half" theory see ref. S22), M06-2X,[S23] M06-HF,[S24] CAM-B3LYP,[S25] LC-$\omega$PBE,[S26] M11,[S27] $\omega$B97,[S28] $\omega$B97X,[S28] $\omega$B97X-D;[S29] CC2[S30] and ADC(2)[S31,S32] with aug-cc-pVDZ basis set,[S33–S35] as well as their spin-component scaled variants SCS and SOS.[S36] The TD-HF and TD-DFT calculations were done with Gaussian 09 (Revision D.01), the CC2 and ADC(2) calculations were performed with TURBOMOLE (Version 6.5).[S37] For the latter the resolution of the identity (RI)[S38,S39] and the frozen core approximations were used. The auxiliary basis set for RI[S40] was also employed. DFT/MRCI calculations were done using TURBOMOLE (Version 6.3).[S41]

The vertical stick spectra were broadened with Gaussian functions:[S42]

$$I(\lambda) = \sum_i f_i \exp\left(-\frac{1}{2\sigma^2}\left(\frac{1}{\lambda} - \frac{1}{\lambda_i}\right)^2\right).$$

Here, $I$ is the absorbance (in arbitrary units), $\lambda$ is the wavelength, $\lambda_i$ and $f_i$ are computed excitation wavelengths and oscillator strengths, respectively, $\sigma$ is a broadening parameter (we chose (arbitrarily) $\sigma = 1500$ cm$^{-1}$).

Excitation energies and oscillator strengths for the first 14 transitions for all the methods are tabulated in Tab. S1 (monomer) and Tab. S2 (dimer). The broadened spectra obtained with AM1/FOMO-CI, DFT/MRCI, TD-HF, TD-M11, CC2, and SCS-CC2 are presented in Fig. S2. In Fig. S2 the experimental wavelength, 301 nm (4.12 eV), is also shown. This wavelength corresponds to the maximal absorption of the *trans*-AB monomer, recorded in gas phase.[S43]

From Fig. S2 it is seen that the semiempirical spectra are energetically close (in terms of a location of the $\pi\pi^*$ absorption band) to the TD-HF ones, showing a blue shift with

respect to other methods and to the available experimental gas-phase result.[S43] At the same time, the difference with modern range-separated density functionals (such as M11 or $\omega$B97) or the wavefunction SCS-CC2 method is not very pronounced ($\sim$0.1–0.25 eV). Moreover, AM1/FOMO-CI shows the presence of doubly excited states, which are also found with DFT/MRCI. For example, on the AM1/FOMO-CI and DFT/MRCI levels the $S_0 \rightarrow S_3$ transition of the dimer has the double $n\pi^*$ character.

More specifically and returning to Tabs. S1 and S2 we note that for the monomer (Tab. S1) all the methods show that the $S_0 \rightarrow S_2$ ($\pi \rightarrow \pi^*$) transition is the first bright transition, with oscillator strength ranging from 0.73 (SOS-CC2) to 0.91 (AM1/FOCI). The excitation energies for this transition are in the interval 3.79 (DFT/MRCI) – 4.59 (M06-HF) eV, *i.e.*, differing maximally by 0.8 eV.

For the dimer (Tab. S2), TD-HF and TD-DFT produce the 4th transition as the first bright transition, while with CC2 and ADC2 methods this first bright transition is the 6th one. AM1/FOMO-CI also shows the first bright transition to be the 6th one, whereas with DFT/MRCI this is the 9th transition. Excitation energies for the first bright state range from 3.72 (DFT/MRCI) to 4.71 (M06-HF) eV, *i.e.*, differ maximally by 1 eV. The oscillator strength for this first bright transition of the dimer ranges from 0.97 (SOS-CC2) to 1.56 (DFT/MRCI). Here we should note that the original DFT/MRCI method[S16] is not suitable for the description of the absorption of the dimeric systems.[S44]

**Table S1: Excitation energies $\Delta E$ and oscillator strengths $f$ of the *trans*-azobenzene monomer**

| | AM1/FOMO-CI | | DFT/MRCI | | HF | | BHandHLYP | | M06-2X | | M06-HF | |
|---|---|---|---|---|---|---|---|---|---|---|---|---|
| Transition | $\Delta E$ (eV) | $f$ | $\Delta E$ (eV) | $f$ | $\Delta E$ (eV) | $f$ | $\Delta E$ (eV) | $f$ | $\Delta E$ (eV) | $f$ | $\Delta E$ (eV) | $f$ |
| $S_0 \rightarrow S_1$ | 3.34 | 0.00 | 2.24 | 0.00 | 3.17 | 0.00 | 2.89 | 0.00 | 2.45 | 0.00 | 2.01 | 0.00 |
| $S_0 \rightarrow S_2$ | **4.39** | **0.91** | **3.79** | **0.88** | **4.43** | **0.77** | **4.12** | **0.83** | **4.16** | **0.84** | **4.59** | **0.87** |
| $S_0 \rightarrow S_3$ | 4.58 | 0.00 | 3.92 | 0.05 | 5.59 | 0.03 | 4.84 | 0.04 | 4.80 | 0.03 | 5.34 | 0.02 |
| $S_0 \rightarrow S_4$ | 4.62 | 0.24 | 3.92 | 0.00 | 5.60 | 0.00 | 4.84 | 0.00 | 4.81 | 0.00 | 5.35 | 0.00 |
| $S_0 \rightarrow S_5$ | 5.33 | 0.00 | 3.96 | 0.00 | 5.87 | 0.00 | 5.51 | 0.00 | 5.54 | 0.00 | 6.17 | 0.00 |
| $S_0 \rightarrow S_6$ | 6.15 | 0.01 | 4.53 | 0.00 | 6.82 | 0.65 | 6.21 | 0.27 | 6.16 | 0.28 | 6.72 | 0.00 |
| $S_0 \rightarrow S_7$ | 6.32 | 0.00 | 4.59 | 0.00 | 7.10 | 0.00 | 6.22 | 0.00 | 6.16 | 0.00 | 6.77 | 0.64 |
| $S_0 \rightarrow S_8$ | 6.33 | 0.02 | 4.61 | 0.00 | 7.11 | 0.82 | 6.49 | 0.00 | 6.33 | 0.00 | 6.82 | 0.00 |
| $S_0 \rightarrow S_9$ | 6.49 | 0.00 | 4.66 | 0.00 | 7.35 | 0.00 | 6.75 | 0.44 | 6.39 | 0.00 | 6.98 | 0.00 |
| $S_0 \rightarrow S_{10}$ | 6.51 | 0.56 | 4.96 | 0.00 | 8.10 | 0.00 | 6.85 | 0.00 | 6.46 | 0.00 | 7.16 | 0.51 |
| $S_0 \rightarrow S_{11}$ | 6.96 | 0.00 | 5.05 | 0.00 | 8.29 | 0.00 | 6.89 | 0.00 | 6.63 | 0.00 | 7.25 | 0.00 |
| $S_0 \rightarrow S_{12}$ | 7.06 | 0.00 | 5.27 | 0.00 | 8.44 | 0.60 | 6.98 | 0.00 | 6.65 | 0.00 | 7.28 | 0.00 |
| $S_0 \rightarrow S_{13}$ | 7.18 | 0.04 | 5.32 | 0.00 | 8.54 | 0.00 | 7.17 | 0.00 | 6.65 | 0.00 | 7.59 | 0.00 |
| $S_0 \rightarrow S_{14}$ | 7.57 | 0.00 | 5.40 | 0.32 | 8.79 | 0.00 | 7.24 | 0.00 | 6.89 | 0.40 | 7.68 | 0.00 |

| | CAM-B3LYP | | LC-$\omega$PBE | | M11 | | $\omega$B97 | | $\omega$B97X | | $\omega$B97X-D | |
|---|---|---|---|---|---|---|---|---|---|---|---|---|
| Transition | $\Delta E$ (eV) | $f$ | $\Delta E$ (eV) | $f$ | $\Delta E$ (eV) | $f$ | $\Delta E$ (eV) | $f$ | $\Delta E$ (eV) | $f$ | $\Delta E$ (eV) | $f$ |
| $S_0 \rightarrow S_1$ | 2.72 | 0.00 | 2.74 | 0.00 | 2.47 | 0.00 | 2.80 | 0.00 | 2.76 | 0.00 | 2.69 | 0.00 |
| $S_0 \rightarrow S_2$ | **4.08** | **0.82** | **4.37** | **0.82** | **4.30** | **0.84** | **4.36** | **0.81** | **4.26** | **0.82** | **4.10** | **0.82** |
| $S_0 \rightarrow S_3$ | 4.72 | 0.03 | 5.09 | 0.02 | 5.02 | 0.03 | 5.09 | 0.02 | 4.98 | 0.03 | 4.74 | 0.03 |
| $S_0 \rightarrow S_4$ | 4.73 | 0.00 | 5.09 | 0.00 | 5.03 | 0.00 | 5.10 | 0.00 | 4.99 | 0.00 | 4.75 | 0.00 |
| $S_0 \rightarrow S_5$ | 5.46 | 0.00 | 5.84 | 0.00 | 5.79 | 0.00 | 5.82 | 0.00 | 5.73 | 0.00 | 5.52 | 0.00 |
| $S_0 \rightarrow S_6$ | 6.12 | 0.26 | 6.59 | 0.46 | 6.45 | 0.40 | 6.58 | 0.47 | 6.42 | 0.39 | 6.16 | 0.28 |
| $S_0 \rightarrow S_7$ | 6.12 | 0.00 | 6.61 | 0.00 | 6.47 | 0.00 | 6.60 | 0.00 | 6.45 | 0.00 | 6.17 | 0.00 |
| $S_0 \rightarrow S_8$ | 6.29 | 0.00 | 6.69 | 0.00 | 6.52 | 0.00 | 6.75 | 0.00 | 6.62 | 0.00 | 6.25 | 0.00 |
| $S_0 \rightarrow S_9$ | 6.30 | 0.00 | 6.89 | 0.46 | 6.80 | 0.00 | 6.86 | 0.46 | 6.77 | 0.00 | 6.25 | 0.00 |
| $S_0 \rightarrow S_{10}$ | 6.37 | 0.00 | 6.90 | 0.00 | 6.88 | 0.00 | 6.88 | 0.00 | 6.82 | 0.43 | 6.33 | 0.00 |
| $S_0 \rightarrow S_{11}$ | 6.51 | 0.00 | 7.06 | 0.00 | 6.88 | 0.00 | 7.10 | 0.00 | 6.83 | 0.00 | 6.57 | 0.00 |
| $S_0 \rightarrow S_{12}$ | 6.74 | 0.37 | 7.11 | 0.00 | 6.91 | 0.00 | 7.14 | 0.00 | 6.89 | 0.00 | 6.74 | 0.37 |
| $S_0 \rightarrow S_{13}$ | 6.76 | 0.00 | 7.13 | 0.00 | 6.93 | 0.44 | 7.18 | 0.00 | 7.01 | 0.00 | 6.74 | 0.00 |
| $S_0 \rightarrow S_{14}$ | 6.80 | 0.00 | 7.26 | 0.00 | 7.00 | 0.00 | 7.31 | 0.00 | 7.10 | 0.00 | 6.75 | 0.00 |

| | CC2 | | ADC(2) | | SCS-CC2 | | SCS-ADC(2) | | SOS-CC2 | | SOS-ADC(2) | |
|---|---|---|---|---|---|---|---|---|---|---|---|---|
| Transition | $\Delta E$ (eV) | $f$ | $\Delta E$ (eV) | $f$ | $\Delta E$ (eV) | $f$ | $\Delta E$ (eV) | $f$ | $\Delta E$ (eV) | $f$ | $\Delta E$ (eV) | $f$ |
| $S_0 \rightarrow S_1$ | 2.83 | 0.00 | 2.84 | 0.00 | 3.01 | 0.00 | 3.02 | 0.00 | 3.09 | 0.00 | 3.10 | 0.00 |
| $S_0 \rightarrow S_2$ | **4.10** | **0.88** | **4.10** | **0.89** | **4.25** | **0.82** | **4.25** | **0.88** | **4.32** | **0.73** | **4.31** | **0.82** |
| $S_0 \rightarrow S_3$ | 4.48 | 0.02 | 4.51 | 0.03 | 4.53 | 0.00 | 4.55 | 0.00 | 4.52 | 0.00 | 4.54 | 0.00 |
| $S_0 \rightarrow S_4$ | 4.49 | 0.00 | 4.52 | 0.00 | 4.54 | 0.06 | 4.56 | 0.07 | 4.56 | 0.14 | 4.57 | 0.14 |
| $S_0 \rightarrow S_5$ | 5.20 | 0.00 | 5.24 | 0.00 | 5.39 | 0.00 | 5.42 | 0.00 | 5.48 | 0.00 | 5.50 | 0.00 |
| $S_0 \rightarrow S_6$ | 5.56 | 0.00 | 5.64 | 0.00 | 5.99 | 0.42 | 6.01 | 0.48 | 6.09 | 0.46 | 6.10 | 0.54 |
| $S_0 \rightarrow S_7$ | 5.66 | 0.00 | 5.73 | 0.00 | 6.03 | 0.00 | 6.05 | 0.00 | 6.13 | 0.00 | 6.15 | 0.00 |
| $S_0 \rightarrow S_8$ | 5.71 | 0.00 | 5.78 | 0.00 | 6.09 | 0.00 | 6.10 | 0.00 | 6.16 | 0.00 | 6.17 | 0.00 |
| $S_0 \rightarrow S_9$ | 5.81 | 0.32 | 5.84 | 0.38 | 6.12 | 0.00 | 6.18 | 0.00 | 6.35 | 0.00 | 6.36 | 0.00 |
| $S_0 \rightarrow S_{10}$ | 5.88 | 0.00 | 5.90 | 0.00 | 6.20 | 0.00 | 6.25 | 0.00 | 6.40 | 0.00 | 6.45 | 0.00 |
| $S_0 \rightarrow S_{11}$ | 5.90 | 0.00 | 5.95 | 0.00 | 6.28 | 0.00 | 6.29 | 0.00 | 6.44 | 0.00 | 6.48 | 0.00 |
| $S_0 \rightarrow S_{12}$ | 5.94 | 0.00 | 5.97 | 0.00 | 6.28 | 0.00 | 6.33 | 0.00 | 6.53 | 0.00 | 6.54 | 0.00 |
| $S_0 \rightarrow S_{13}$ | 5.96 | 0.08 | 6.02 | 0.04 | 6.40 | 0.00 | 6.45 | 0.00 | 6.55 | 0.00 | 6.60 | 0.00 |
| $S_0 \rightarrow S_{14}$ | 6.06 | 0.03 | 6.15 | 0.01 | 6.48 | 0.03 | 6.49 | 0.00 | 6.60 | 0.00 | 6.60 | 0.00 |

**Table S2: Excitation energies $\Delta E$ and oscillator strengths $f$ of the *trans*-azobenzene–*trans*-azobenzene dimer at the monomer separation of 3.5 Å**

| | AM1/FOMO-CI | | DFT/MRCI | | HF | | BHandHLYP | | M06-2X | | M06-HF | |
|---|---|---|---|---|---|---|---|---|---|---|---|---|
| Transition | $\Delta E$ (eV) | $f$ | $\Delta E$ (eV) | $f$ | $\Delta E$ (eV) | $f$ | $\Delta E$ (eV) | $f$ | $\Delta E$ (eV) | $f$ | $\Delta E$ (eV) | $f$ |
| $S_0 \rightarrow S_1$ | 3.02 | 0.00 | 1.90 | 0.00 | 3.14 | 0.00 | 2.83 | 0.00 | 2.39 | 0.00 | 1.98 | 0.00 |
| $S_0 \rightarrow S_2$ | 3.04 | 0.00 | 1.94 | 0.00 | 3.17 | 0.00 | 2.87 | 0.00 | 2.43 | 0.00 | 2.00 | 0.00 |
| $S_0 \rightarrow S_3$ | 3.75 | 0.00 | 2.40 | 0.00 | 3.95 | 0.00 | 3.44 | 0.00 | 3.46 | 0.00 | 4.05 | 0.00 |
| $S_0 \rightarrow S_4$ | 4.01 | 0.00 | 3.06 | 0.00 | **4.57** | **1.31** | **4.26** | **1.40** | **4.29** | **1.41** | **4.71** | **1.47** |
| $S_0 \rightarrow S_5$ | 4.56 | 0.00 | 3.41 | 0.00 | 5.21 | 0.00 | 4.32 | 0.00 | 4.30 | 0.00 | 4.96 | 0.00 |
| $S_0 \rightarrow S_6$ | **4.57** | **1.53** | 3.42 | 0.00 | 5.22 | 0.00 | 4.33 | 0.00 | 4.30 | 0.00 | 4.97 | 0.00 |
| $S_0 \rightarrow S_7$ | 4.57 | 0.00 | 3.53 | 0.00 | 5.47 | 0.00 | 4.49 | 0.01 | 4.49 | 0.02 | 5.34 | 0.03 |
| $S_0 \rightarrow S_8$ | 4.74 | 0.00 | 3.53 | 0.00 | 5.60 | 0.03 | 4.84 | 0.06 | 4.80 | 0.04 | 5.35 | 0.00 |
| $S_0 \rightarrow S_9$ | 4.74 | 0.00 | **3.72** | **1.56** | 5.61 | 0.00 | 4.85 | 0.00 | 4.81 | 0.00 | 5.64 | 0.00 |
| $S_0 \rightarrow S_{10}$ | 4.89 | 0.00 | 3.86 | 0.05 | 5.93 | 0.00 | 4.92 | 0.00 | 4.87 | 0.00 | 5.97 | 0.00 |
| $S_0 \rightarrow S_{11}$ | 4.94 | 0.33 | 3.86 | 0.00 | 6.31 | 0.00 | 4.97 | 0.00 | 4.89 | 0.00 | 6.05 | 0.00 |
| $S_0 \rightarrow S_{12}$ | 5.39 | 0.01 | 3.90 | 0.00 | 6.38 | 0.00 | 5.28 | 0.00 | 4.93 | 0.00 | 6.12 | 0.00 |
| $S_0 \rightarrow S_{13}$ | 5.49 | 0.01 | 3.91 | 0.00 | 6.42 | 0.00 | 5.30 | 0.00 | 4.97 | 0.00 | 6.22 | 0.00 |
| $S_0 \rightarrow S_{14}$ | 5.57 | 0.00 | 4.01 | 0.01 | 6.45 | 0.00 | 5.46 | 0.00 | 5.39 | 0.00 | 6.28 | 0.00 |

| | CAM-B3LYP | | LC-$\omega$PBE | | M11 | | $\omega$B97 | | $\omega$B97X | | $\omega$B97X-D | |
|---|---|---|---|---|---|---|---|---|---|---|---|---|
| Transition | $\Delta E$ (eV) | $f$ | $\Delta E$ (eV) | $f$ | $\Delta E$ (eV) | $f$ | $\Delta E$ (eV) | $f$ | $\Delta E$ (eV) | $f$ | $\Delta E$ (eV) | $f$ |
| $S_0 \rightarrow S_1$ | 2.65 | 0.00 | 2.69 | 0.00 | 2.42 | 0.00 | 2.75 | 0.00 | 2.70 | 0.00 | 2.62 | 0.00 |
| $S_0 \rightarrow S_2$ | 2.69 | 0.00 | 2.73 | 0.00 | 2.46 | 0.00 | 2.78 | 0.00 | 2.74 | 0.00 | 2.66 | 0.00 |
| $S_0 \rightarrow S_3$ | 3.43 | 0.00 | 3.88 | 0.00 | 3.78 | 0.00 | 3.83 | 0.00 | 3.71 | 0.00 | 3.48 | 0.00 |
| $S_0 \rightarrow S_4$ | **4.22** | **1.37** | **4.50** | **1.40** | **4.43** | **1.44** | **4.48** | **1.38** | **4.38** | **1.39** | **4.23** | **1.38** |
| $S_0 \rightarrow S_5$ | 4.27 | 0.00 | 4.77 | 0.00 | 4.67 | 0.00 | 4.73 | 0.00 | 4.60 | 0.00 | 4.32 | 0.00 |
| $S_0 \rightarrow S_6$ | 4.27 | 0.00 | 4.77 | 0.00 | 4.68 | 0.00 | 4.74 | 0.00 | 4.61 | 0.00 | 4.33 | 0.00 |
| $S_0 \rightarrow S_7$ | 4.48 | 0.02 | 5.09 | 0.03 | 5.03 | 0.04 | 5.10 | 0.03 | 4.98 | 0.03 | 4.58 | 0.01 |
| $S_0 \rightarrow S_8$ | 4.72 | 0.03 | 5.10 | 0.00 | 5.04 | 0.00 | 5.11 | 0.00 | 4.99 | 0.00 | 4.71 | 0.00 |
| $S_0 \rightarrow S_9$ | 4.73 | 0.00 | 5.42 | 0.00 | 5.20 | 0.00 | 5.36 | 0.00 | 5.19 | 0.00 | 4.72 | 0.00 |
| $S_0 \rightarrow S_{10}$ | 4.73 | 0.02 | 5.54 | 0.00 | 5.34 | 0.00 | 5.53 | 0.00 | 5.25 | 0.00 | 4.74 | 0.04 |
| $S_0 \rightarrow S_{11}$ | 4.75 | 0.00 | 5.81 | 0.00 | 5.51 | 0.00 | 5.84 | 0.00 | 5.48 | 0.00 | 4.75 | 0.00 |
| $S_0 \rightarrow S_{12}$ | 4.91 | 0.00 | 5.85 | 0.00 | 5.57 | 0.00 | 5.87 | 0.00 | 5.48 | 0.00 | 4.99 | 0.00 |
| $S_0 \rightarrow S_{13}$ | 4.93 | 0.00 | 5.88 | 0.00 | 5.59 | 0.00 | 5.90 | 0.00 | 5.56 | 0.00 | 5.01 | 0.00 |
| $S_0 \rightarrow S_{14}$ | 5.42 | 0.00 | 5.89 | 0.00 | 5.84 | 0.00 | 5.92 | 0.00 | 5.77 | 0.00 | 5.50 | 0.00 |

| | CC2 | | ADC(2) | | SCS-CC2 | | SCS-ADC(2) | | SOS-CC2 | | SOS-ADC(2) | |
|---|---|---|---|---|---|---|---|---|---|---|---|---|
| Transition | $\Delta E$ (eV) | $f$ | $\Delta E$ (eV) | $f$ | $\Delta E$ (eV) | $f$ | $\Delta E$ (eV) | $f$ | $\Delta E$ (eV) | $f$ | $\Delta E$ (eV) | $f$ |
| $S_0 \rightarrow S_1$ | 2.69 | 0.00 | 2.71 | 0.00 | 2.91 | 0.00 | 2.92 | 0.00 | 3.00 | 0.00 | 3.02 | 0.00 |
| $S_0 \rightarrow S_2$ | 2.77 | 0.00 | 2.78 | 0.00 | 2.97 | 0.00 | 2.98 | 0.00 | 3.07 | 0.00 | 3.08 | 0.00 |
| $S_0 \rightarrow S_3$ | 3.36 | 0.00 | 3.39 | 0.00 | 3.61 | 0.00 | 3.62 | 0.00 | 3.73 | 0.00 | 3.73 | 0.00 |
| $S_0 \rightarrow S_4$ | 3.96 | 0.00 | 3.99 | 0.00 | 4.11 | 0.00 | 4.13 | 0.00 | 4.15 | 0.00 | 4.16 | 0.00 |
| $S_0 \rightarrow S_5$ | 3.97 | 0.00 | 4.00 | 0.00 | 4.11 | 0.00 | 4.13 | 0.00 | 4.16 | 0.00 | 4.17 | 0.00 |
| $S_0 \rightarrow S_6$ | **4.15** | **1.48** | **4.15** | **1.50** | **4.32** | **1.27** | **4.32** | **1.40** | **4.38** | **0.97** | **4.38** | **1.14** |
| $S_0 \rightarrow S_7$ | 4.42 | 0.03 | 4.45 | 0.04 | 4.49 | 0.00 | 4.51 | 0.00 | 4.50 | 0.00 | 4.51 | 0.00 |
| $S_0 \rightarrow S_8$ | 4.42 | 0.00 | 4.46 | 0.00 | 4.52 | 0.22 | 4.53 | 0.22 | 4.56 | 0.51 | 4.57 | 0.51 |
| $S_0 \rightarrow S_9$ | 4.45 | 0.00 | 4.54 | 0.00 | 4.83 | 0.00 | 4.85 | 0.00 | 4.94 | 0.00 | 4.96 | 0.00 |
| $S_0 \rightarrow S_{10}$ | 4.51 | 0.01 | 4.57 | 0.01 | 4.95 | 0.00 | 4.98 | 0.00 | 5.18 | 0.00 | 5.20 | 0.00 |
| $S_0 \rightarrow S_{11}$ | 4.51 | 0.00 | 4.60 | 0.00 | 5.19 | 0.00 | 5.26 | 0.00 | 5.36 | 0.00 | 5.36 | 0.00 |
| $S_0 \rightarrow S_{12}$ | 4.59 | 0.00 | 4.62 | 0.00 | 5.22 | 0.00 | 5.27 | 0.00 | 5.46 | 0.00 | 5.46 | 0.00 |
| $S_0 \rightarrow S_{13}$ | 5.00 | 0.00 | 5.04 | 0.00 | 5.25 | 0.00 | 5.30 | 0.00 | 5.57 | 0.00 | 5.48 | 0.00 |
| $S_0 \rightarrow S_{14}$ | 5.06 | 0.00 | 5.08 | 0.00 | 5.33 | 0.00 | 5.35 | 0.00 | 5.59 | 0.00 | 5.60 | 0.00 |

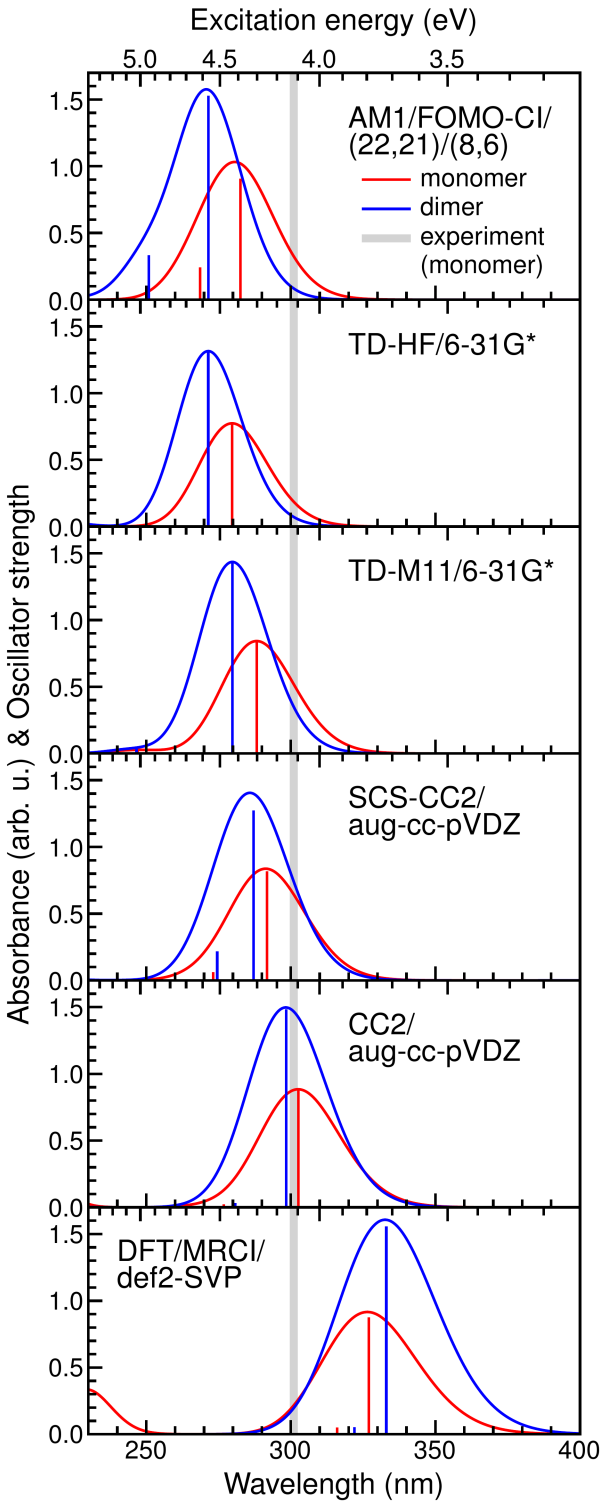


Figure S2: Broadened and stick vertical absorption spectra of the monomer and the dimer calculated with various methods. Grey thick line represents experimentally detected gas-phase wavelength of maximal absorption, for the monomer.[S43]

Next, we see that the dimerization causes small spectral shift ($\lesssim$ 0.2 eV), mainly to the blue with exception of DFT/MRCI (see also Figs. S2 and S3), and the increase of the oscillator strength of the bright transition. This shift can be explained in terms of the molecular exciton theory, which predicts the splitting of the bright state in two states, the upper of which is allowed and the lower forbidden for a dimer composed of two identical monomers located side by side, as it is for our model — so-called *exciton* or *Davydov splitting*. The excitation energies of the split states in the dimer are $\Delta E_{\pm,dimer} = \Delta E_{monomer} \pm \frac{\Delta\mathcal{E}_{exciton}}{2} + \Delta D$.[S45,S46] Here $\Delta E_{monomer}$ is the excitation energy of the bright transition for the monomer, $\Delta\mathcal{E}_{exciton}$ exciton splitting in the dimer, $\Delta D$ van der Waals correction. Usually $\Delta D < 0$, that leads to the red shift of the splitting origin relative to the monomer excitation energy.

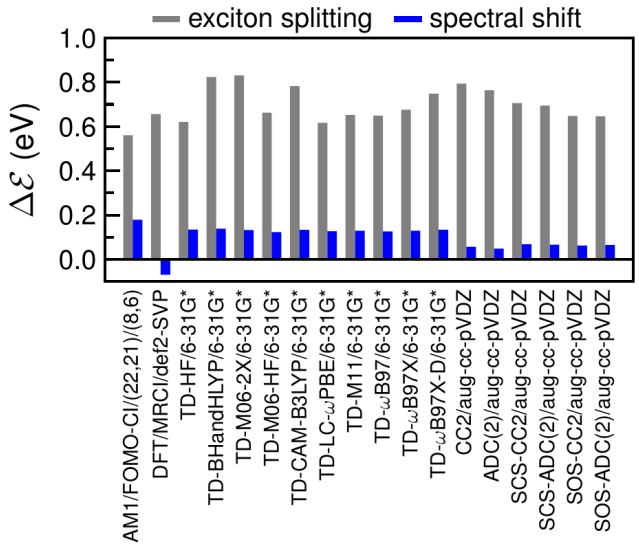


Figure S3: $\Delta\mathcal{E}_{exciton} = \Delta E_{+,dimer} - \Delta E_{-,dimer}$ and $\Delta\mathcal{E}_{shift} = \Delta E^{bright}_{dimer} - \Delta E^{bright}_{monomer}$ ($\Delta E^{bright}_{dimer} = \Delta E_{+}$).

We determined the exciton splitting from our first-principles calculations based on analysis of canonical and/or natural transition orbitals of the lowest transitions, up to the bright one.[S42] The splitting turned out to be $\gtrsim$ 0.6 eV (Fig. S3). The excitation energy differences corresponding to the exciton splitting of the bright transition are shown in

Tab. S3. It is also interesting to note that the found method dependence of the exciton splitting (Fig. S3) is quite moderate, however, it is more pronounced than for the tilted 4-nitroazobenzene dimer studied by us recently.[S42]

**Table S3: Excitation energy differences used to calculate the exciton splitting**

| Method | Excitation energy difference |
|---|---|
| AM1/FOMO-CI | $\Delta E_6 - \Delta E_4$ |
| DFT/MRCI | $\Delta E_9 - \Delta E_4$ |
| TD-HF | $\Delta E_4 - \Delta E_3$ |
| TD-DFT | $\Delta E_4 - \Delta E_3$ |
| (SCS/SOS-)CC2, ADC(2) | $\Delta E_6 - \Delta E_3$ |

Finally, the absorption spectrum of the "SAM" model differs from the spectrum of the dimer, as it should be expected from the molecular exciton theory. We demonstrate this by using the TD-HF/6-31G* method calculating the spectrum of all twelve molecules of the "SAM" together (this approach can be refered to as the supermolecule approach). The result is shown in Fig. S4. In the monomer the bright transition at this level of theory is $S_0 \rightarrow S_2$. In the dimer, in agreement with the exciton theory, the bright transition is $S_0 \rightarrow S_4$, *i.e.*, the first monomer excited state splits into two states in the dimer as well as the second (bright) monomer excited state does. In the "SAM" model the bright (the most intense) transition is $S_0 \rightarrow S_{24}$, that corresponds to the splitting of the second excited state of the monomer into 12 excited states of the "SAM" (and the splitting of the monomer first excited state into 12 states in the "SAM"). The bright transition in the "SAM" is blue-shifted by $\sim$0.25 eV in comparison to the dimer, the oscillator strength is $\sim$3.8 times larger.

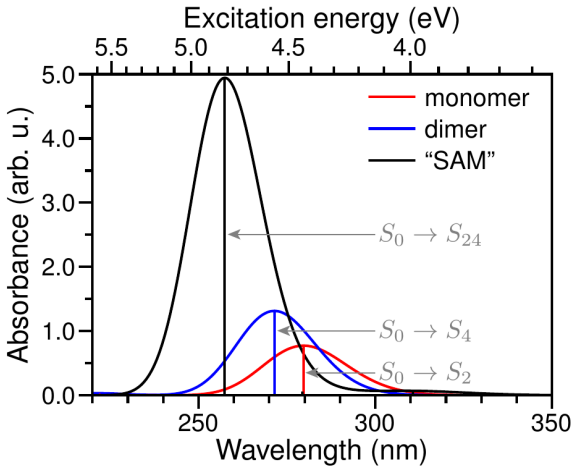


Figure S4: Broadened and stick vertical absorption spectra of the monomer, the dimer, and the "SAM" model calculated with the TD-HF/6-31G* method. The bright transitions are labeled.

## CN and NN bond torsions during Brownian and photodynamics

### Brownian dynamics

The oscillator strength of the $n\pi^*$ transition ($S_0 \rightarrow S_1$) of *trans*-AB was shown to markedly depend on CN bond torsions of the phenyl rings and, to smaller extent, on the torsion of the NN bond.[S47] To explain the difference in the intensity of the $n\pi^*$ bands between the studied systems (see Fig. 2 (b) of the main text), we tracked the NNCC as well as CNNC dihedrals (see Fig. S5 for the definition of the angles) during the Brownian dynamics. The time-averaged values are presented in Tab. S4. From Tab. S4 it is seen that the molecules become on average more planar (bigger mean values of the dihedrals), meaning the smaller oscillator strength, when going from the monomer over the dimer to the "SAM". This explains why we do not observe the enhancement of the absorption for the dimer in comparison to the monomer, as it would be expected from the exciton theory. Moreover, this explains the very weak absorption of the "SAM". Also note that the standard deviations of the dihedrals decrease with model complexity.

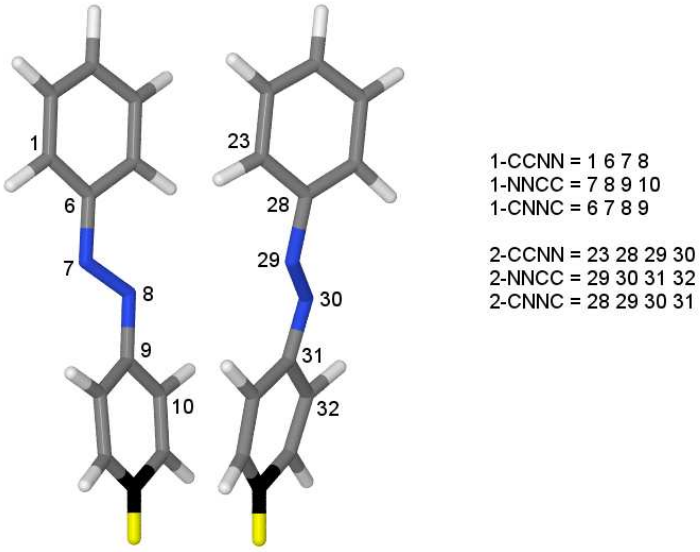


Figure S5: Definition of the dihedral NNCC and CNNC angles. Fixed carbon atoms are shown in black, fixed hydrogen atoms in yellow. The geometry corresponds to the end of the Brownian trajectory for the isolated dimer.

**Table S4: Time-averaged dihedral NNCC and CNNC angles (in degrees) for the Brownian trajectories**

| Angle | Monomer | Dimer | "SAM" |
|---|---|---|---|
| 1-CCNN | $164 \pm 14$ | $167 \pm 10$ | $171 \pm 7$ |
| 1-NNCC | $166 \pm 11$ | $168 \pm 9$ | $172 \pm 6$ |
| 1-CNNC | $175 \pm 4$ | $175 \pm 4$ | $176 \pm 3$ |
| 2-CCNN | | $165 \pm 11$ | $169 \pm 9$ |
| 2-NNCC | | $167 \pm 10$ | $168 \pm 9$ |
| 2-CNNC | | $175 \pm 4$ | $176 \pm 3$ |

## Photodynamics

Below we present the time evolution of the ensemble-averaged NNCC and CNNC dihedrals (Fig. S6) as well as the $n\pi^*$–$\pi\pi^*$ ($E_4 - E_3$) energy gap (Fig. S7) for the dimer and the "SAM", while trajectories travel in any of the states of the $\pi\pi^*$ manifold. All trajectories (reacitve, unreactive, and undetermined) were considered for this analysis. Note that, in general, the number of trajectories in the ensemble (used for averaging) depends on the time.

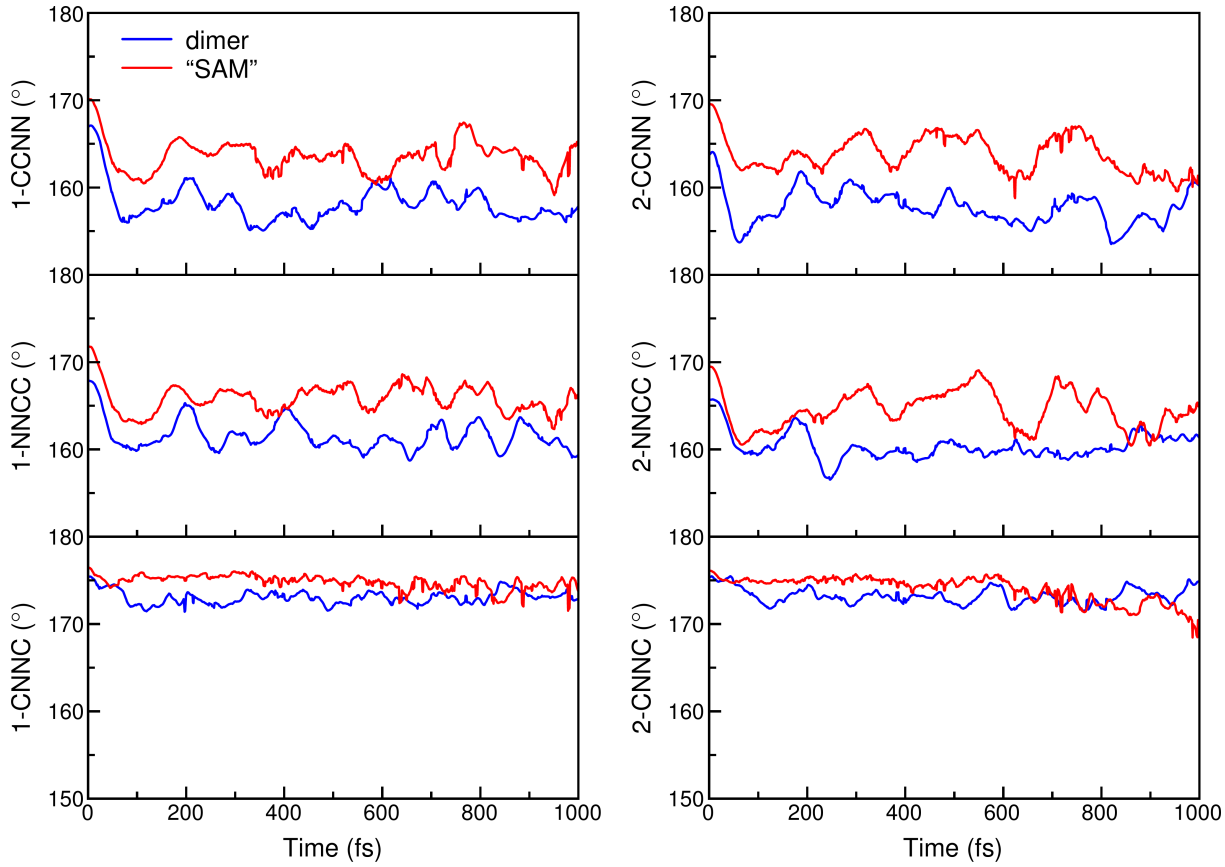


Figure S6: Time evolution of the ensemble-averaged NNCC and CNNC dihedrals, while trajectories are on any of the surfaces of the $\pi\pi^*$ manifold.

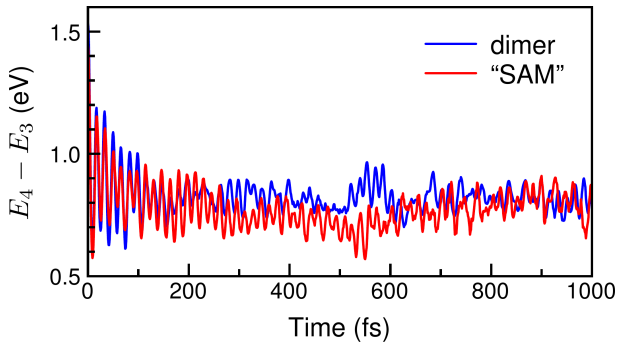


Figure S7: Time evolution of the ensemble-averaged $E_4 - E_3$ energy gap, while trajectories are on any of the surfaces of the $\pi\pi^*$ manifold.

## References


(S1) Becke, A. D. Density-Functional Thermochemistry. III. The Role of Exact Exchange. *J. Chem. Phys.* **1993**, *98*, 5648–5652.

(S2) Stephens, P. J.; Devlin, F. J.; Chabalowski, C. F.; Frisch, M. J. Ab Initio Calculation of Vibrational Absorption and Circular Dichroism Spectra Using Density Functional Force Fields. *J. Phys. Chem.* **1994**, *98*, 11623–11627.

(S3) Hehre, W. J.; Ditchfield, R.; Pople, J. A. Self-Consistent Molecular Orbital Methods. XII. Further Extensions of Gaussian-Type Basis Sets for Use in Molecular Orbital Studies of Organic Molecules. *J. Chem. Phys.* **1972**, *56*, 2257–2261.

(S4) Hariharan, P.; Pople, J. The Influence of Polarization Functions on Molecular Orbital Hydrogenation Energies. *Theor. Chim. Acta* **1973**, *28*, 213–222.

(S5) Frisch, M. J.; Trucks, G. W.; Schlegel, H. B.; Scuseria, G. E.; Robb, M. A.; Cheeseman, J. R.; Scalmani, G.; Barone, V.; Mennucci, B.; Petersson, G. A. et al. Gaussian 09, Revision D.01. Gaussian Inc., Wallingford CT, 2009.

(S6) Dewar, M. J. S.; Zoebisch, E. G.; Healy, E. F.; Stewart, J. J. P. Development and Use of Quantum Mechanical Molecular Models. 76. AM1: A New General Purpose Quantum Mechanical Molecular Model. *J. Am. Chem. Soc.* **1985**, *107*, 3902–3909.

(S7) Cusati, T.; Granucci, G.; Martínez-Núñez, E.; Martini, F.; Persico, M.; Vázquez, S. Semiempirical Hamiltonian for Simulation of Azobenzene Photochemistry. *J. Phys. Chem. A* **2012**, *116*, 98–110.

(S8) Granucci, G.; Toniolo, A. Molecular Gradients for Semiempirical {CI} Wavefunctions with Floating Occupation Molecular Orbitals. *Chem. Phys. Lett.* **2000**, *325*, 79–85.

(S9) Granucci, G.; Persico, M.; Toniolo, A. Direct Semiclassical Simulation of

Photochemical Processes with Semiempirical Wave Functions. *J. Chem. Phys.* **2001**, *114*, 10608–10615.

(S10) Ciminelli, C.; Granucci, G.; Persico, M. Are Azobenzenophanes Rotation-Restricted? *J. Chem. Phys.* **2005**, *123*, 174317.

(S11) Stewart, J. J. P. MOPAC 2002, Fujitsu Ltd., Tokyo, Japan.

(S12) Floß G.; Saalfrank, P. The Photoinduced $E \rightarrow Z$ Isomerization of Bisazobenzenes: A Surface Hopping Molecular Dynamics Study. *J. Phys. Chem. A* **2015**, *119*, 5026–5037.

(S13) Lii, J. H.; Allinger, N. L. Molecular Mechanics. The MM3 Force Field for Hydrocarbons. 3. The van der Waals' Potentials and Crystal Data for Aliphatic and Aromatic Hydrocarbons. *J. Am. Chem. Soc.* **1989**, *111*, 8576–8582.

(S14) Tai, J. C.; Yang, L.; Allinger, N. L. Molecular Mechanics (MM3). Calculations on Nitrogen-Containing Aromatic Heterocycles. *J. Am. Chem. Soc.* **1993**, *115*, 11906–11917.

(S15) Ponder, J. W. TINKER 6.1; Washington University School of Medicine: St. Louis, MO, 2012, (http://dasher.wustl.edu/tinker).

(S16) Grimme, S.; Waletzke, M. A Combination of Kohn–Sham Density Functional Theory and Multi-Reference Configuration Interaction Methods. *J. Chem. Phys.* **1999**, *111*, 5645–5655.

(S17) Schäfer, A.; Horn, H.; Ahlrichs, R. Fully Optimized Contracted Gaussian Basis Sets for Atoms Li to Kr. *The Journal of Chemical Physics* **1992**, *97*, 2571–2577.

(S18) Weigend, F.; Ahlrichs, R. Balanced Basis Sets of Split Valence, Triple Zeta Valence and Quadruple Zeta Valence Quality for H to Rn: Design and Assessment of Accuracy. *Phys. Chem. Chem. Phys.* **2005**, *7*, 3297–3305.

(S19) Dreuw, A.; Head-Gordon, M. Single-Reference Ab Initio Methods for the Calculation of Excited States of Large Molecules. *Chem. Rev.* **2005**, *105*, 4009–4037.

(S20) Casida, M.; Huix-Rotllant, M. Progress in Time-Dependent Density-Functional Theory. *Annu. Rev. Phys. Chem.* **2012**, *63*, 287–323.

(S21) Casida, M. *Time-Dependent Density Functional Response Theory for Molecules. Recent Advances in Density Functional Methods*; World Scientific, 1995; Chapter 5, pp 155–192.

(S22) Becke, A. D. A New Mixing of Hartree–Fock and Local Density-Functional Theories. *J. Chem. Phys.* **1993**, *98*, 1372–1377.

(S23) Zhao, Y.; Truhlar, D. The M06 Suite of Density Functionals for Main Group Thermochemistry, Thermochemical Kinetics, Noncovalent Interactions, Excited States, and Transition Elements: Two New Functionals and Systematic Testing of Four M06-Class Functionals and 12 Other Functionals. *Theor. Chem. Acc.* **2008**, *120*, 215–241.

(S24) Zhao, Y.; ; Truhlar, D. G. Density Functional for Spectroscopy:No Long-Range Self-Interaction Error, Good Performance for Rydberg and Charge-Transfer States, and Better Performance on Average than B3LYP for Ground States. *J. Phys. Chem. A* **2006**, *110*, 13126–13130.

(S25) Yanai, T.; Tew, D. P.; Handy, N. C. A New Hybrid Exchange-Correlation Functional Using the Coulomb-Attenuating Method (CAM-B3LYP). *Chem. Phys. Lett.* **2004**, *393*, 51–57.

(S26) Vydrov, O. A.; Scuseria, G. E. Assessment of a Long-Range Corrected Hybrid Functional. *J. Chem. Phys.* **2006**, *125*, 234109.

(S27) Peverati, R.; Truhlar, D. G. Improving the Accuracy of Hybrid Meta-GGA Density Functionals by Range Separation. *J. Phys. Chem. Lett.* **2011**, *2*, 2810–2817.

(S28) Chai, J.-D.; Head-Gordon, M. Systematic Optimization of Long-Range Corrected Hybrid Density Functionals. *J. Chem. Phys.* **2008**, *128*, 084106.

(S29) Chai, J.-D.; Head-Gordon, M. Long-Range Corrected Hybrid Density Functionals with Damped Atom–Atom Dispersion Corrections. *Phys. Chem. Chem. Phys.* **2008**, *10*, 6615–6620.

(S30) Christiansen, O.; Koch, H.; Jørgensen, P. The Second-Order Approximate Coupled Cluster Singles and Doubles Model CC2. *Chem. Phys. Lett.* **1995**, *243*, 409–418.

(S31) Schirmer, J. Beyond the Random-Phase Approximation: A New Approximation Scheme for the Polarization Propagator. *Phys. Rev. A* **1982**, *26*, 2395–2416.

(S32) Trofimov, A. B.; Schirmer, J. An Efficient Polarization Propagator Approach to Valence Electron Excitation Spectra. *J. Phys. B: At., Mol. Opt. Phys.* **1995**, *28*, 2299–2324.

(S33) Dunning, T. H. Gaussian Basis Sets for Use in Correlated Molecular Calculations. I. The Atoms Boron through Neon and Hydrogen. *J. Chem. Phys.* **1989**, *90*, 1007–1023.

(S34) Kendall, R. A.; Dunning, T. H.; Harrison, R. J. Electron Affinities of the First-Row Atoms Revisited. Systematic Basis Sets and Wave Functions. *J. Chem. Phys.* **1992**, *96*, 6796–6806.

(S35) Woon, D. E.; Dunning, T. H. Gaussian Basis Sets for Use in Correlated Molecular Calculations. III. The Atoms Aluminum through Argon. *J. Chem. Phys.* **1993**, *98*, 1358–1371.

(S36) Hellweg, A.; Grün, S. A.; Hättig, C. Benchmarking the Performance of Spin-Component Scaled CC2 in Ground and Electronically Excited States. *Phys. Chem. Chem. Phys.* **2008**, *10*, 4119–4127.

(S37) TURBOMOLE V6.5 2013, a development of University of Karlsruhe and Forschungszentrum Karlsruhe GmbH, 1989-2007, TURBOMOLE GmbH, since 2007; available from `http://www.turbomole.com`.

(S38) Hättig, C.; Weigend, F. CC2 Excitation Energy Calculations on Large Molecules Using the Resolution of the Identity Approximation. *J. Chem. Phys.* **2000**, *113*, 5154–5161.

(S39) Hättig, C.; Köhn, A. Transition Moments and Excited-State First-Order Properties in the Coupled-Cluster Model CC2 Using the Resolution-of-the-Identity Approximation. *J. Chem. Phys.* **2002**, *117*, 6939–6951.

(S40) Weigend, F.; Köhn, A.; Hättig, C. Efficient Use of the Correlation Consistent Basis Sets in Resolution of the Identity MP2 Calculations. *J. Chem. Phys.* **2002**, *116*, 3175–3183.

(S41) TURBOMOLE V6.3 2011, a development of University of Karlsruhe and Forschungszentrum Karlsruhe GmbH, 1989-2007, TURBOMOLE GmbH, since 2007; available from `http://www.turbomole.com`.

(S42) Titov, E.; Saalfrank, P. Exciton Splitting of Adsorbed and Free 4-Nitroazobenzene Dimers: A Quantum Chemical Study. *J. Phys. Chem. A* **2016**, *120*, 3055–3070.

(S43) Andersson, J.-Å.; Petterson, R.; Tegnér, L. Flash Photolysis Experiments in the Vapour Phase at Elevated Temperatures I: Spectra of Azobenzene and the Kinetics of Its Thermal *cis-trans* Isomerization. *J. Photochem.* **1982**, *20*, 17–32.

(S44) Lyskov, I.; Kleinschmidt, M.; Marian, C. M. Redesign of the DFT/MRCI Hamiltonian. *J. Chem. Phys.* **2016**, *144*, 034104.

(S45) Davydov, A. S. The Theory of Molecular Excitons. *Soviet Physics Uspekhi* **1964**, *7*, 145–178.

(S46) Kasha, M.; Rawls, H.; Ashraf El-Bayoumi, M. The Exciton Model in Molecular Spectroscopy. *Pure Appl. Chem.* **1965**, *11*, 371–392.

(S47) Cusati, T.; Granucci, G.; Persico, M.; Spighi, G. Oscillator Strength and Polarization of the Forbidden $n \rightarrow \pi^*$ Band of *trans*-Azobenzene: A Computational Study. *J. Chem. Phys.* **2008**, *128*, 194312.